Title

Assessment of co-sintering as a fabrication approach for metal-supported proton-conducting solid oxide cells

Authors

Wang, Ruofan
Byrne, Conor
Tucker, Michael C

Publication Date

2019-04-01

DOI

10.1016/j.ssi.2019.01.004

Peer reviewed

Assessment of Co-Sintering as a Fabrication Approach for Metal-Supported Proton-Conducting Solid Oxide Cells

Ruofan Wang[1], Conor Byrne[1], Michael C. Tucker[1,*]

[1] Energy Conversion Group, Energy Storage and Distributed Resources Division, Lawrence Berkeley National Laboratory, Berkeley, California, United States

* Corresponding author: Michael C. Tucker, mctucker@lbl.gov, Tel +1 (510) 486-5304, 1 Cyclotron Road, MS 62-203, Berkeley, CA 94720, United States

Abstract

Proton conducting oxide electrolyte materials could potentially lower the operating temperature of metal-supported solid oxide cells (MS-SOCs) to the intermediate range 400 to 600 °C. The porous metal substrate provides the advantages of MS-SOCs such as high thermal and redox cycling tolerance, low-cost of structural materials, and mechanical ruggedness. In this work, viability of co-sintering fabrication of metal-supported proton conducting solid oxide cells is investigated. Candidate proton conducting oxides including perovskite oxides $BaZr_{0.7}Ce_{0.2}Y_{0.1}O_{3-\delta}$, $SrZr_{0.5}Ce_{0.4}Y_{0.1}O_{3-\delta}$, and $Ba_3Ca_{1.18}Nb_{1.82}O_{9-\delta}$, pyrochlore oxides $La_{1.95}Ca_{0.05}Zr_2O_{7-\delta}$ and $La_2Ce_2O_7$, and acceptor doped rare-earth ortho-niobate $La_{0.99}Ca_{0.01}NbO_4$ are synthesized via solid state reactive or sol-gel methods. These ceramics are sintered at 1450 °C in reducing environment alone and supported on Fe-Cr alloy metal support, and their key characteristics such as phase formation, sintering property, and chemical compatibility with

metal support are determined. Most electrolyte candidates suffer from one or more challenges identified for this fabrication approach, including: phase decomposition in reducing atmosphere, evaporation of electrolyte constituents, contamination of the electrolyte with Si and Cr from the metal support, and incomplete electrolyte sintering. In contrast, $La_{0.99}Ca_{0.01}NbO_4$ is found to be highly compatible with the metal support and co-sintering processing in reducing atmosphere. A metal-supported cell is fabricated with $La_{0.99}Ca_{0.01}NbO_4$ electrolyte, ferritic stainless steel support, Pt air electrode and nanoparticulate ceria-Ni hydrogen electrocatalyst. The total resistance is 50 $\Omega \cdot cm^2$ at 600 °C. This work clearly demonstrates the challenges, opportunities, and breakthrough of metal-supported proton-conducting solid oxide cells by co-sintering fabrication.

Keywords: Protonic ceramic fuel cells; Metal supported; Protonic ceramic electrochemical cells; Doped barium zirconate; Doped strontium zirconate; Ca doped lanthanum ortho-niobate

1. Introduction

Proton-conducting oxide ceramics are widely explored as alternatives to conventional oxide conductors, primarily because the proton conductors display higher conductivity at intermediate temperatures (400-600 °C). A number of reviews covering proton conducting materials and their applications are available [1-9]. Use of proton conducting electrolytes in solid oxide fuel cells (SOFCs) and electrolysis cells (SOECs) enables efficient operation at lower temperatures, reducing thermal stress and allowing the use of less expensive stack materials and balance-of-plant components. Transport of protons across the electrolyte offers other advantages at all

temperatures: for electrolysis, pure hydrogen is produced so steam does not need to be removed from the product stream; for fuel cell operation, extraction of hydrogen from the anode through the electrolyte can drive fuel decomposition or reforming reactions forward. Protonic ceramic fuel cells (PCFCs) furthermore resist carbon coking and are tolerant to sulfur, enabling stable operation with a wide variety of hydrocarbon fuels [10, 11]. Proton conductors are also the basis for sensors and other electrochemical processes, including ammonia synthesis [12], hydrogen electrochemical compression [13], hydrogen separation [4, 14], and conversion of CO_2 to CH_4 [15].

Metal-supported solid oxide fuel cells (MS-SOFCs) incorporate thin layers of electrochemically-active ceramics supported on thicker metal layers that provide mechanical support and electronic current collection. MS-SOFCs promise high performance provided by the active ceramic layers, and excellent mechanical properties and low materials cost derived from the metal support. In contrast to conventional all-ceramic SOFCs, MS-SOFCs offer further operational advantages including; mechanical ruggedness; tolerance to very rapid thermal cycling both during start-up and variable operation [16, 17]; and tolerance to oxidation of the fuel catalyst, which occurs during high fuel utilization, intermittent fuel use, or unexpected loss of fuel supply (i.e. due to failure in the fuel delivery subsystem) [18, 19]. Because of these cost and operational advantages, MS-SOFCs are being developed for applications that require fast-start or intermittent operation, including personal power generators [17, 20, 21], residential combined heat and power [19], vehicle range extenders [22-24], and electrolysis cells for conversion of variable power sources such as wind and solar [25-27]. Details of MS-SOFC materials selection, cell architecture, processing approaches, and notable cell and system demonstrations are available in

various review articles [28-30]. Ferritic stainless steel is a typical choice for the metal support, as it displays good oxidation resistance below about 800 °C, has a coefficient of thermal expansion that is similar to common SOFC ceramic materials, and is very inexpensive compared to other alloys with similar corrosion resistance. Our group has extensive experience developing MS-SOFCs and MS-SOECs with oxide-conducting ceramics and ferritic supports based on P434L stainless steel, and therefore that alloy is selected for the screening and initial cell development effort reported here [16, 18, 22, 27, 31].

Given the advantages of PCFCs and MS-SOFCs discussed above, it is of interest to develop metal-supported protonic ceramic electrochemical cells. Figure 1 illustrates metal-supported protonic ceramic cells operating in fuel cell and electrolysis conditions. To date, the preliminary work in this nascent field is limited to the use of barium cerium yttrium zirconate (BZCY) type materials as the electrolyte. Mercadelli et al. co-sintered BZCY-Ni anodes supported on ferritic stainless steel, finding that interdiffusion between the anode and steel layers was a significant issue and resulted in contamination of the Ni catalyst and melting of the stainless steel [32]. Although the authors were successful in minimizing interdiffusion via addition of a ceria barrier layer, a complete cell was not fabricated. Recently, Stange et al. successfully prepared a complete half-cell on ferritic stainless steel support, with barium yttrium zirconate-Ni (BZY-Ni) electrode and BZY electrolyte deposited by pulsed laser deposition (PLD) [33, 34]. Under electrolysis conditions (hydrogen vs. steam), the cell displayed a high total resistance of 40 $Ohm \cdot cm^2$ at 600 °C, indicating that significant optimization effort remains to achieve the performance expected for a BZY-based cell.

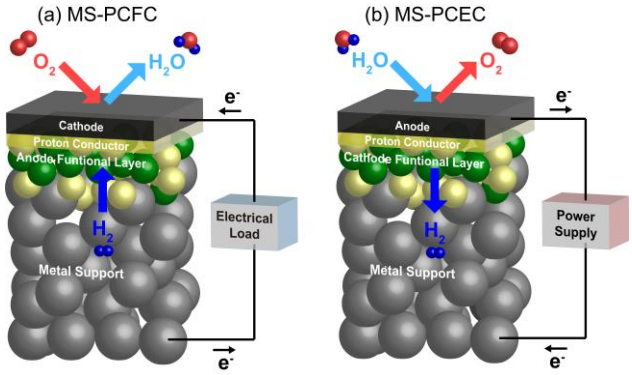

Figure 1. Cell architecture. Schematic representation of (a) metal supported protonic ceramic fuel cell (MS-PCFC), and (b) metal supported protonic ceramic electrolysis cell (MS-PCEC). Only a thin portion of the hydrogen electrode layer, as required for electrochemical function, is retained in the MSC design.

Figure 2 shows the conductivities of representative proton conductors [11, 35-43]. While BZCY-type materials are the most-studied proton conductors for PCFCs due to their high conductivity, other proton conductors may be more compatible with the metal-supported cell architecture, materials set, and processing constraints. Co-sintering a ceramic layer on stainless steel is challenging, in part because reducing sintering atmosphere is required to prevent oxidation of the steel. Processing oxide ceramics in reducing atmosphere may cause decomposition, impart oxygen non-stoichiometry, exacerbate evaporation of various elements, or result in poor sintering. Contact with the metal support may further cause undesirable interdiffusion between the layers. Identifying proton conducting ceramics that are compatible with this processing approach is a primary goal of this work. It is anticipated that if a compatible family of proton-conducting oxides is identified, other limitations such as low conductivity or high sintering temperature can be overcome with focused effort. For barium cerium yttrium zirconate (BZCY) as an example, conductivity has been improved almost an order of magnitude (see Figure 2), and

sintering temperature has dropped from approximately 1600 °C to 1350 °C after several years of global effort focused on doping and powder processing improvements [11, 35, 44, 45]. Here, we select representative compositions from several families of proton-conducting oxides and determine their suitability for co-sintering on stainless steel. Initially, we assess whether they are compatible with (a) reducing atmosphere sintering and (b) direct contact with metal support during sintering. More detailed studies for the compatible compositions then include interdiffusion, densification behavior, evaporation during sintering. Finally, thin layers of proton conductors supported on porous steel supports are prepared and electrochemically tested.

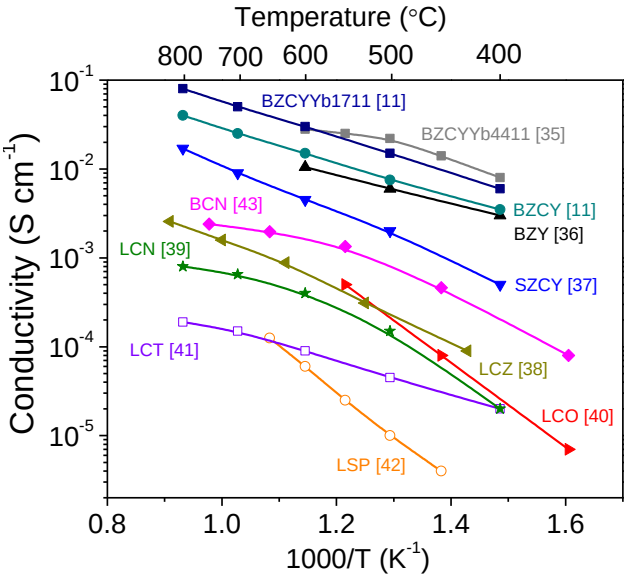

Figure 2. Conductivities of representative proton conductors. Data are reproduced from [11, 35-43].

2. Experimental

2.1.Materials synthesis

Candidate proton-conducting ceramics including perovskite oxides $BaZr_{0.7}Ce_{0.2}Y_{0.1}O_{3-\delta}$ (BZCY), $SrZr_{0.5}Ce_{0.4}Y_{0.1}O_{3-\delta}$ (SZCY), and $Ba_3Ca_{1.18}Nb_{1.82}O_{9-\delta}$ (BCN), pyrochlore oxides

$La_{1.95}Ca_{0.05}Zr_2O_{7-\delta}$ (LCZ) and $La_2Ce_2O_7$ (LCO), and acceptor doped rare-earth ortho-niobate $La_{0.99}Ca_{0.01}NbO_4$ (LCN) were investigated in this study. BZCY was commercially purchased from CerPoTech, Norway [46]. For other compositions, solid state reaction and/or sol-gel methods were used to synthesize the powders.

(a) Solid state reaction method: SZCY, BCN, LCO, and LCN powders were successfully synthesized through solid state reaction. Applicable oxides and carbonates ($SrCO_3$ (Alfa Aesar, 99.99%), ZrO_2 (Alfa Aesar, 99.978%), CeO_2 (Alfa Aesar, 99.99%), Y_2O_3 (Alfa Aesar, 99.99%), $BaCO_3$ (Johnson Matthey Materials, 99.999%), $CaCO_3$ (Alfa Aesar, 99.99%), Nb_2O_5 (Alfa Aesar, 99.99%), and La_2O_3 (JT Baker, >98%)) were mixed in stoichiometric proportions and milled with 1 mm zirconia balls in isopropyl alcohol for 24 hours. La_2O_3 powder was calcined at 900 °C for 10 hours immediately before weighing to decompose hydroxide and carbonate. After ball milling, the suspensions were dried on a stir plate under a heat lamp. The resulting powder precursors were then calcined in air in the temperature range of 1050 to 1400 °C for duration of 5 to 10 hours. Details of solid state reaction synthesis can be found in Table S1. We also attempted to synthesize $La_{1.95}Ca_{0.05}Zr_2O_{7-\delta}$ (LCZ) via the solid state reaction route described in Ref. [38], but the correct phase was not obtained.

(b) Sol-gel method: Since $La_{1.95}Ca_{0.05}Zr_2O_{7-\delta}$ (LCZ) was not successfully synthesized by the solid state reaction route, sol-gel method was used. Stoichiometric amounts of $La(NO_3)_3 \cdot 6H_2O$ (Sigma Aldrich, 99.99%), $Ca(NO_3)_2 \cdot 4H_2O$ (Acros Organics, ≥99%), and $ZrO(NO_3)_2 \cdot xH_2O$ (Sigma Aldrich, 99%) were mixed with citric acid ($HOC(COOH)(CH_2COOH)_2 \cdot H_2O$, Sigma Aldrich, ≥99%) in deionized water. Citric acid/metal molar ratio was 1:1. The solution was stirred and heated on a hot plate at 80 °C until a viscous liquid was obtained. The viscous liquid was then dried in an oven at 100 °C for 5 h, followed by 110 °C for 5 h, until a porous solid mass

was obtained. The solid mass was ground in an agate mortar and calcined at 900 °C for 5 h, after which fine LCZ powder was formed. Similar sol-gel method was also used to successfully obtain fine powders of SZCY, BCN, and LCN. Details of sol-gel synthesis can be found in Table S1.

2.2.Dilatometry and sintering properties

After powders of proton conductors were synthesized and phases were confirmed with X-ray diffraction (XRD), the powders were pressed into pellets with fish oil and polyvinyl butyral as binders (diameter of ~6.35 mm, thickness of ~2 mm). The sintering behaviors of the pellets were examined using a vertical dilatometer (Linseis L75). Uniaxial shrinkage of the pellets was measured as a function of temperature up to 1450 °C, in both dry air or 2% H_2-Ar (reducing) environments.

The pellets were also sintered in air (muffle furnace) or reducing environment (Al_2O_3 tube furnace with 2% H_2-Ar flow), without any compression. The shrinkage, weight loss via evaporation, and sintered density of the pellets were obtained by measuring the dimensions and weight before and after sintering. The sintered pellets were examined by scanning electron microscopy (SEM) and energy X-ray dispersive spectroscopy (EDS) to evaluate their grain size, porosity, and composition change.

2.3.Compatibility of proton conductors with metal

To evaluate the compatibility with the metal support during co-sintering, powders of the proton conductors were mixed with acrylic paint medium (Liquitex) brushed onto bisque fired metal support (P434L Stainless Steel, Ametek, fired at 1050 °C in reducing atmosphere to obtain some mechanical strength). The resulting bilayers were then fired in air at 525 °C to remove acrylic

and then sintered in reducing atmosphere (2% H_2-Ar) at 1450 °C for 2 h. The ceramic layers were then analyzed with SEM, EDS and XRD, in order to image microstructures and determine the extent of composition change or element interdiffusion.

2.4.Metal-supported cell fabrication and electrochemical testing

Complete metal-supported half-cells were fabricated with LCN, SZCY, and BZCY electrolytes and electrode backbones. Commercially available ferritic stainless steel P434L alloy (water atomized, Ametek Specialty Metal Products) with composition of 17 wt.% Cr, 0.20 wt.% Mn, 1.0 wt.% Mo, 0.010 wt.% P, 0.90 wt.% Si, 0.020 wt.% S, 0.020 wt.% C and the balance in Fe, was used as the metal support material. A green metal support sheet was tape-cast and cut into 30mm diameter circles using a laser cutter (Hobby model, Full Spectrum Laser). The circular supports were fired in a box furnace at 525 °C for 1 h to remove the binder and pore former and bisque fired in a tube furnace at 1050 °C for 2 h with 2% H_2-Ar flowing (reducing environment) to provide mechanical integrity for further ceramic deposition. Three layers of selected protonic ceramic powders were applied sequentially, including (a) a hand-painted porous bridging layer for bridging the pores on the metal support surface and providing a smoother surface for subsequent layers, (b) a hand-painted porous electrode layer with fine pores for catalyst infiltration and obtaining a smooth surface for electrolyte deposition, and (c) an aerosol sprayed dense electrolyte. Details of deposition procedures of electrode and electrolyte layers are provided in Supplementary Note 1. After the deposition of the ceramic layers, cells were fired in air at 525 °C for 1 h to remove acrylic, pore formers, and residual solvent. Cells were then sintered at various sintering temperatures for 2 h in 2% H_2-Ar environment.

Cells with dense and crack-free electrolyte (confirmed by surface SEM and leak test with ethanol) were subjected to electrochemical testing. SDC mixed with 20 vol.% Ni (SDCN catalyst) was infiltrated into the pores of the hydrogen electrode using precursor solutions of nitrate salts, with the help of mild vacuum. Details of infiltration can be found in [22, 47, 48]. On top of the electrolyte, Pt paste was painted as air electrode (with area of ~0.9 cm^2) and fired at 850 °C for 30 min. Pt mesh and wires were used for current application and voltage probing. For electrochemical testing, the cell was mounted on an alumina tube with ceramic paste (Ceramabond 552, Aremco). After the ceramic paste was cured, 3% humidified hydrogen (50 sccm) was flowed to the SDCN infiltrated electrode to reduce NiO to Ni. The Pt electrode was exposed to ambient air. Cell impedance was measured as a function of temperature, using electrochemical impedance spectroscopy (EIS) at open-circuit condition (with amplitude of 5 mV, from 200 kHz to 100 mHz) using a potentiostat (Biologic VMP3).

2.5.Materials Characterization

The proton conductor phases after calcination, air sintering, reducing atmosphere sintering, and co-sintered on metal-support were examined by XRD using a Bruker D2 PHASER X-ray diffractometer with CuKα radiation. The ceramic pellets and metal-supported cells were characterized by SEM (Hitachi TM-1000 or JEOL JSM-7500F) and EDS (Thermo Scientific).

3. Results and Discussion

As candidates for co-sintering with ferritic stainless steel, we selected proton conducting oxides with (a) reported sintering temperature in the range 1200 to 1600 °C to be close to the sintering temperature range for ferritic stainless steel of 1250 to 1500 °C, and (b) conductivity of

approximately 10^{-3} S cm^{-1} or higher at 700 °C to enable reasonable resistance for an electrolyte layer of at least several microns thickness that can be produced by low-cost methods such as screen printing or tape casting, see Figure 2. The specific selected compositions are listed in Table 1. BZCY, LCN, LCO, and BCN have been successfully integrated into an operating fuel cell [2, 49-55], and various BZCY and SZCY compositions have been used in steam electrolysis cells [3, 56]. LCZ was demonstrated in an ammonia synthesis cell [57]. To date, none of these have been demonstrated in a co-sintered metal-supported cell.

Table 1. Summary of screening results for proton conductors suitable for co-sintering fabrication of metal supported cells.

Family	Candidate	Representative Composition	Survives sintering in reducing atmosphere?	Survives re-oxidation?	React with Metal?	Densifies at 1450 °C or lower?	Evaporation during sintering?
Pyrochlore	LCZ	$La_{1.95}Ca_{0.05}Zr_2O_7$	NO	NO	-	-	-
	LCO	$La_2Ce_2O_7$	NO	YES	YES – Cr, Si	-	-
Perovskite	BCN	$Ba_3Ca_{1.18}Nb_{1.82}O_9$	YES	YES	YES – Cr, Si	Falls apart	YES
	BZCY	$BaZr_{0.7}Ce_{0.2}Y_{0.1}O_3$	YES	YES	YES – Cr, Si	Marginal	YES
	SZCY	$SrZr_{0.5}Ce_{0.4}Y_{0.1}O_3$	YES	YES	YES - Si	YES	YES
Acceptor doped rare-earth ortho-niobate	LCN	$La_{0.99}Ca_{0.01}NbO_4$	YES	YES	NO	YES	NO

The approach taken here is rapid down-selection from the list of candidates, screening for compatibility with processing conditions and contact with stainless steel metal support as discussed in Sections 3.1-3.3. Compositions that show a major limitation at each stage of screening are removed from further consideration. Table 1 summarizes the screening effort.

3.1.Compatibility with sintering in reducing atmosphere

Starting powders were prepared by solid state reaction, with the exception of BZCY (purchased commercially) and LCZ. For LCZ, the correct phase was not obtained by solid state reaction in the range 1100 to 1400 °C, so it was prepared by sol-gel synthesis instead. XRD confirms that

the intended phase was obtained for each of the fresh powders after synthesis, as the peak patterns are consistent with previous literature, see Figure 3 [37, 43, 50, 57-59].The SZCY powder also contains minor CeO_2 and SrY_2O_4 impurity phases. The peak splitting for BCN is consistent with previous work, where it was suggested that hydrated and dehydrated phases coexist at 1200 °C and heating to 1300 °C and above completely dehydrates the material resulting in single peaks [43].

A high sintering temperature is desirable for ceramic densification, but the porous metal support will over-densify near the melting point of the stainless steel (~1525 °C). Therefore, a nominal sintering temperature of 1450 °C was selected for screening. This is 100 °C higher than the sintering temperature used for YSZ-stainless steel cells [16, 18, 22], but still results in adequate porosity in the metal layer as will be shown in Section 3.4. Pellets of the ceramic powders were exposed to reducing atmosphere at 1450 °C to assess phase stability in the sintering conditions, and to air for comparison. Ideally, the desired phase remains after sintering in both air and reducing exposure, and this is found to be the case for BZCY, SZCY, BCN, and LCN. Both LCO and LCZ showed significant decomposition to constituent oxides when exposed to reducing atmosphere, Figure 3. It is possible to anneal the decomposed ceramics in air to regain the correct phase, however this re-oxidation step is limited to exposure at 850 °C or lower, to avoid oxidation of the metal support in a complete cell. Re-oxidizing LCO in air at 850 °C did indeed recover the correct phase, although the pellet shattered, presumably due to volume expansion arising from oxygen uptake. In contrast, LCZ remained decomposed after re-oxidation, and therefore was eliminated from further consideration.

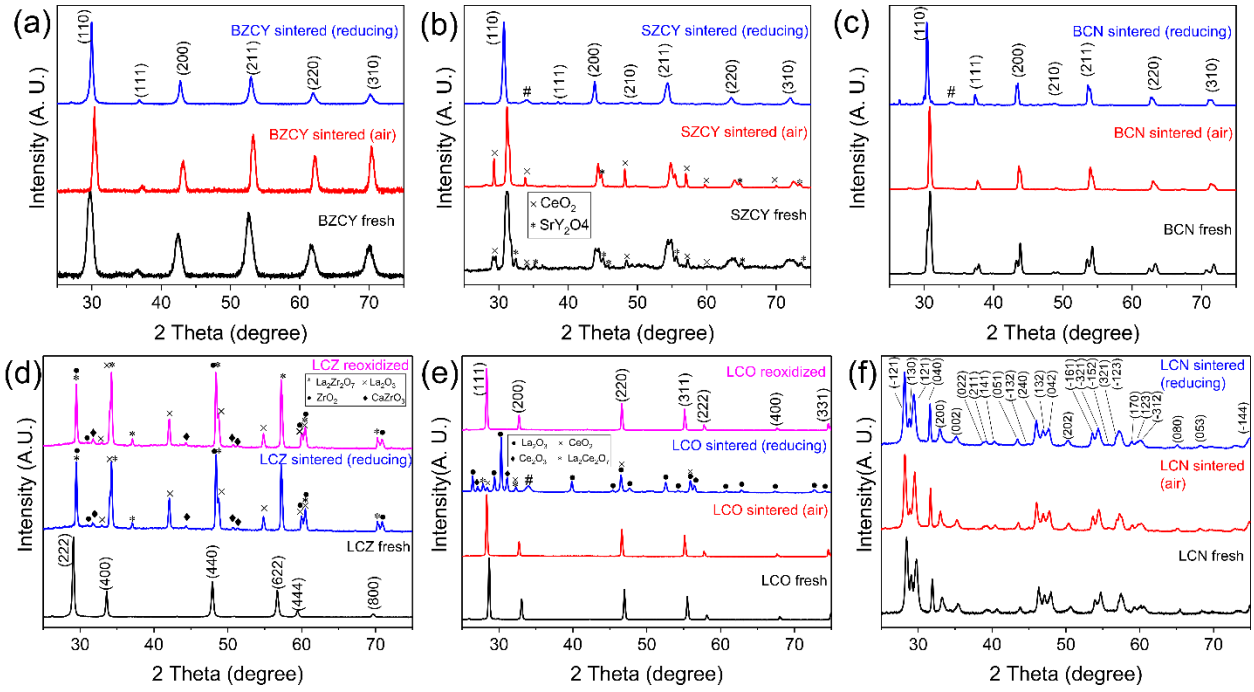

Figure 3. Phase analysis. XRD patterns of powders as synthesized (fresh), after air sintering at 1450 °C, and after reducing atmosphere sintering at 1450 °C: (a) BZCY, (b) SZCY, (c) BCN, (d) LCZ, (e) LCO, and (f) LCN. The desired phases for LCZ and LCO were not obtained after reducing atmosphere sintering, and these were therefore re-oxidized in air at 850 °C. Peaks arising from the sample holder are indicated by "#".

3.2.Reactivity with metal during sintering

The remaining candidates were assessed for reactivity with stainless steel under sintering conditions. Thin layers of ceramic powder were painted onto metal supports, and co-sintered at 1450 °C in reducing atmosphere. Evaporative loss of ceramic cations and diffusion of elements from the metal into the ceramic were determined with EDS (Figure 4a-e), and reaction product phases on the surface of the ceramic were determined with XRD (Figure 4f-j). Ba and Sr loss is observed for BZCY, SZCY, and BCN, as evidenced by a decrease in Ba or Sr EDS peak intensity after sintering these compositions. This is consistent with previous reports of Ba loss

during sintering of barium zirconate via evaporation, which is detrimental to proton conductivity [60, 61]. In addition to Fe and Cr, 434 stainless steel contains Mo, Si, and Mn. Si diffused into BZCY, forming Ba_2SiO_4 on the surface of the ceramic, Figure 4f. Cr diffusion was also observed, although it was limited to the region close to the metal: Y-Cr and Ce-Cr rich phases (presumably $YCrO_3$ and $CeCrO_3$) were detected near the metal with EDS but did not appear in the surface XRD analysis. Similarly for SZCY, Sr_2SiO_4 was observed on the surface of the ceramic (Figure 4g), and for BCN, Ba_2SiO_4 and $BaCrO_4$ were observed (Figure 4h). Interdiffusion of Si and Cr is clearly an issue for BZCY, SZCY, and BCN, although the desired proton-conducting phases were still dominant after co-sintering. In contrast, LCO reacted completely with the metal. Upon decomposition to La-oxide and Ce-oxide (see Section 3.1), the La-oxide further reacts with Cr and Si from the metal, forming $La_{9.33}Si_6O_{26}$ and $LaCrO_3$; no residual LCO phase is observed (Figure 4i). LCO was therefore eliminated from further consideration. LCN is the only composition that survives reducing atmosphere, does not lose cations to evaporation, and did not react with the metal support.

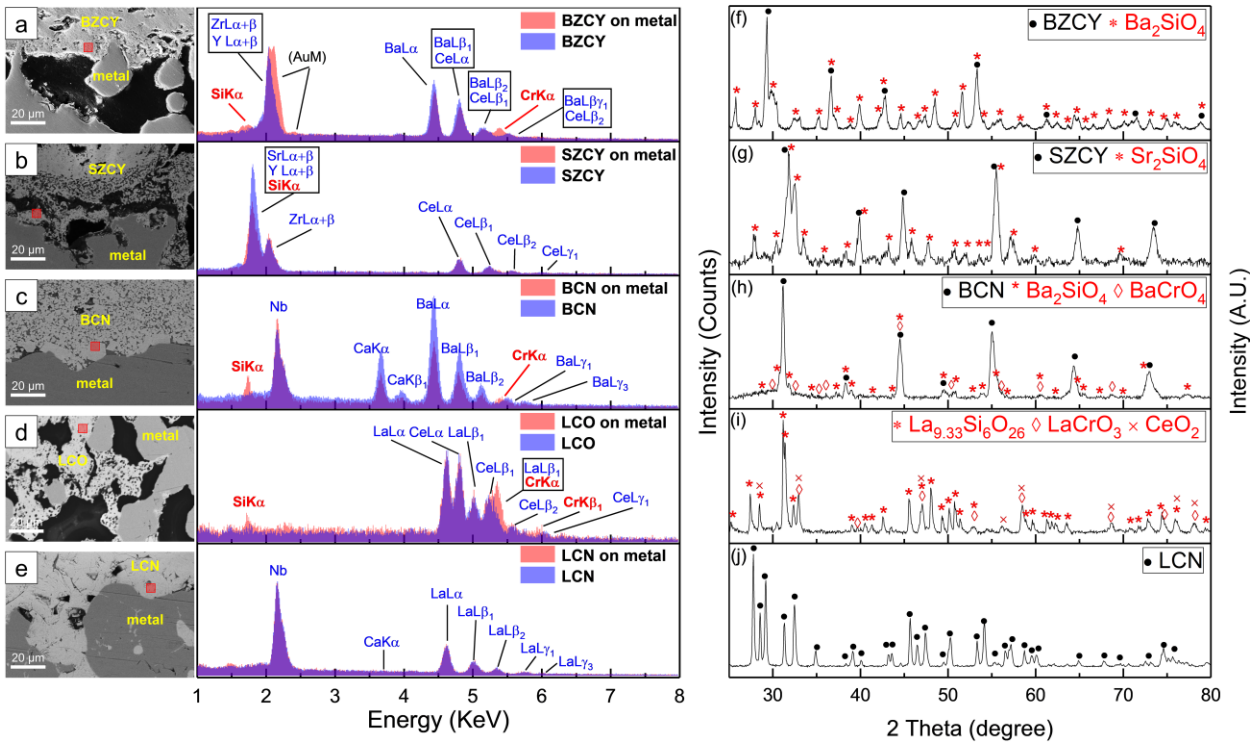

Figure 4. Compositional and phase stability after co-sintering on metal support. SEM images and corresponding EDS area analyses of proton conductors sintered on metal support: (a) BZCY, (b) SZCY, (c) BCN, (d) LCO, and (e) LCN. EDS analyses were conducted in areas close to metal support, as illustrated in SEM images. Surface XRD patterns of proton conductors: (f) BZCY, (g) SZCY, (h) BCN, (i) LCO, and (j) LCN.

3.3.Densification behavior

For compatibility with co-sintering on metal support, the ceramic layer will ideally densify completely at 1450 °C or below, with shrinkage somewhat less than the bare metal (~20%) [31] and minimal change in composition due to evaporation. Pellets of the remaining candidate ceramics were sintered in reducing atmosphere to determine general densification and evaporation behavior, see Table 2. BCN showed low shrinkage, and high weight loss due to Ba evaporation during sintering (Ba evaporation is identified by EDS, see Figure S1). The sintered

BCN pellet was only 57% dense, and disintegrated into powder within hours of being removed from the sintering furnace. Therefore, BCN was eliminated from further consideration. BZCY showed suitable shrinkage and moderate loss of Ba, but only achieved 73% densification. Significant residual porosity is evident in the microstructure of the sintered pellet, Figure 5a. This is not surprising, as BZCY is typically sintered at 1500-1600 °C. Recent work indicates that addition of sintering aids, modification of the composition, and use of a reactive sintering approach can all lead to complete densification in air below 1500 °C [44, 45, 62]. Therefore, we anticipate that with future effort these approaches will enable densification in reducing atmosphere as well. LCN and SZCY both showed suitable shrinkage and achieved almost complete densification. SZCY displayed moderate evaporation of Sr (see Table 2 and Figure S1), whereas LCN did not experience weight loss during sintering. The sintered SZCY and LCN pellets had well-formed micron-scale grains and minimal residual porosity, Figure 5b and 5c.

Table 2. Sintering behavior. Shrinkage, weight loss, and density of pellets after sintering in reducing atmosphere (2% H_2-Ar) at 1450 °C for 2 h. Sintering properties of pellets in air can be seen in Table S2.

Composition	Shrinkage (%)	Weight loss (%)	Sintered density (g/cm^3)	Density (% of theor.)
BZCY	18	6	4.5	73 [a]
SZCY	14	9	5.3	97 [b]
BCN	6	17	3.2	57 [c]
LCN	19	0	5.8	99 [d]

[a] Provided by CerPoTech, Norway [46].

[b] Calculated from unit cell data in [43].

[c] Calculated from unit cell data in [37].

[d] Average of undoped and 2% Ca doped $LaNbO_4$ in [59].

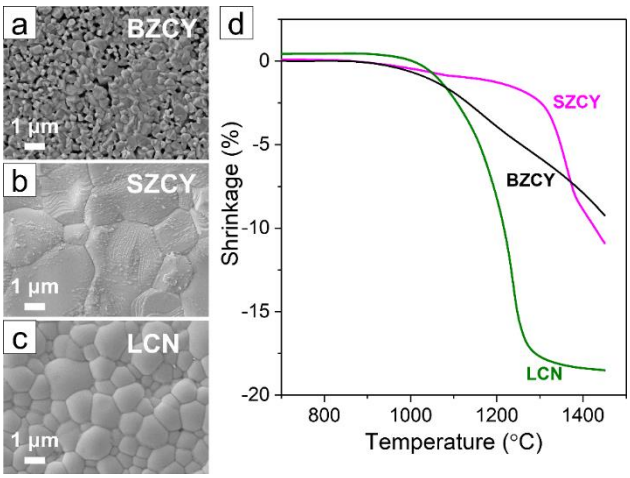

Figure 5. (a-c) Sintered microstructure. Surface SEM micrographs of (a) BZCY, (b) SZCY, and (c) LCN pellets after sintering in reducing atmosphere (2% H_2-Ar) at 1450 °C for 2 h. **(d) Sintering profiles.** Dilatometry of BZCY, SZCY, and LCN pellets sintered in reducing atmosphere (2% H_2-Ar) up to 1450 °C.

To further elucidate sintering behavior, dilatometry of BZCY, SZCY, and LCN was conducted in reducing atmosphere, Figure 5d. BZCY sintering starts around 900 °C and continues gradually to 1450 °C. A plateau indicating completion of sintering is not observed, consistent with the residual porosity and incomplete densification discussed above. SZCY sintering is delayed relative to BZCY, but proceeds quickly above about 1300 °C. LCN shows a classic sintering curve, with incipient sintering around 950 °C, followed by continuous shrinkage leading to a plateau indicating that sintering is nearly complete at 1300 °C and above. This result prompted the sintering temperature study discussed below in Section 3.4. In general, the sintering behavior of these materials in reducing atmosphere is quite similar to that in air, as shown in Figure S2. Sintering is delayed by about 50 °C in reducing atmosphere for both SZCY and LCN, and minimal impact is seen for BZCY.

In summary, the sintering behavior of SZCY and LCN appear to be compatible with co-sintering on metal support, and BZCY is expected to be suitable as well with some additional effort.

3.4.Metal-supported electrolyte layers

Because SZCY and LCN have good sinterability at temperature ≤ 1450 °C, they were selected for metal-supported cell fabrication. Cell fabrication with BZCY was also attempted despite incomplete densification at 1450 °C (see Section 3.3) because of its higher proton conductivity.

Figure 6 shows the cross-sectional SEM images of the cells based on BZCY and SZCY. EDS spectra obtained from the indicated points/areas are provided in Figure S3. The cell microstructure can be summarized as follows:

(a) BZCY: Cr and Si diffusion from metal support was identified to be the main issue for BZCY. EDS analysis obtained in the vicinity of metal support shows this area is enriched with Ce, Y, Cr, and almost Ba and Zr depleted, Figure S3f. In the area close to BZCY surface, amount of Cr becomes smaller, Figure S3e. In addition to Cr, minor Si diffusion was also observed throughout the BZCY layers, with a concentration of ~1 atomic %, Figure S3e and S3f. It is also worth-mentioning that BZCY co-sintered with metal support was found to be surprisingly denser than BZCY pellet, although some cracks were observed in the electrolyte. The denser structure of BZCY layers may result from co-shrinking of the metal support, which enhances the densification of co-sintered BZCY layers. Cr and Si, although considered to be detrimental, could act as reactive sintering aids.

(b) SZCY: After co-sintering, a significant penetration of ceramic layers into the metal support was observed and porosity in the metal support became very small, Figure S3b. Significant Si diffusion from metal support was observed. At least three different phases can be

distinguished by SEM/EDS: a Si, Ce-rich brighter phase (Figure S3g), a Si, Sr-rich darker phase (Figure S3h), and a Sr, Zr-rich (Ce-deficient) brighter phase with hexagonal structure (Figure S3i). Cr diffusion was smaller in SZCY compared to BZCY (minor Cr was observed in Figure S3i).

Since BZCY and SZCY were found to react with the metal support during co-sintering, further cell fabrication and testing with these two materials were not pursued.

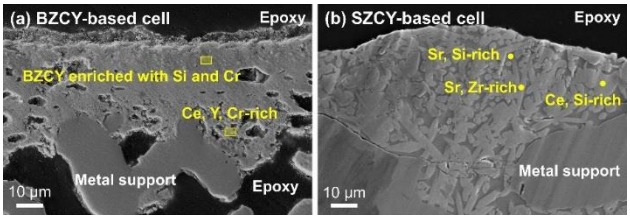

Figure 6. Co-sintered BZCY and SZCY cells. Cell structure with (a) BZCY and (b) SZCY electrode-electrolyte after sintering at 1450 °C. EDS spectra obtained from the indicated points are provided in Figure S3.

LCN does not react with the metal support and can be sintered at temperature lower than 1450 °C. To obtain a cell structure with dense electrolyte and appropriate porosities of the metal support and electrode backbone (for catalyst infiltration and gas diffusion), the sintering temperature for LCN-based cells was varied from 1250 to 1450 °C, Figure S4. 1300 °C was found to be optimal, providing a dense electrolyte with thickness of ~10 µm and metal support with porosity of ~36% (estimated using ImageJ software), Figure 7. In comparison, the cell sintered at 1250 °C shows cracks in the electrolyte and minimal sintered connection within the metal support (Figure S4a-b), and cells sintered at 1350 °C or higher show agglomeration and pore-filling of LCN in the metal support and significant densification of the metal support

(Figure S4e-j). Therefore, 1300 °C was chosen to be the best sintering temperature for LCN-based cell.

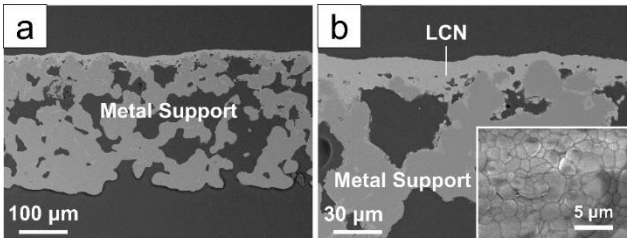

Figure 7. Co-sintered LCN cell. Cell structure with LCN electrode-electrolyte after sintering at 1300 °C. Inset image shows the surface morphology of the LCN electrolyte.

3.5.Electrochemcial testing of LCN-based metal-supported cell

Fabrication was completed for a LCN-based cell sintered at 1300 °C, by infiltrating SDCN catalyst into the LCN backbone on the metal support side, and applying Pt paste on the LCN electrolyte. The single cell has diameter of 25 mm and active area of 0.9 cm^2. Initial electrochemical testing was performed in the range 450 to 750 °C. The open-circuit voltage (OCV) at 700 °C was approximately 1.02 V, which is lower than the theoretical value of 1.12 V, suggesting some leakage through the electrolyte of the present cell, but higher than the values reported in the literature for cells based on LCN electrolyte [49, 52]. Figure 8a shows the ohmic, polarization and total impedance of the cell as a function of temperature, determined with EIS. At 600 °C, the ohmic resistance (R_Ω) and total resistance (R_{total}) were approximately 30 and 50 $\Omega \cdot cm^2$, respectively (Figure 8b). Based on a thickness of 10 µm, the conductivity of metal supported LCN electrolyte was calculated to be approximately 3.7×10^{-4} S cm^{-1} at 600 °C, which is in agreement with the values of pellets reported in the literature [39, 59]. The relatively large R_Ω is ascribed to the low conductivity of LCN and could be reduced by decreasing electrolyte thickness or improving conductivity via doping. The polarization resistance (R_p) was smaller

than R_Ω below 650 °C, and plateaued above 650 °C. In this work, Pt paste was used as the electrode on the air side and SDCN catalyst from high temperature SOFC was adopted on the fuel side. R_p can be further reduced if improved materials are used as the oxygen and hydrogen catalysts. Note that we did not observe an obvious discontinuity in area specific resistance (ASR) related to the phase transition between monoclinic at lower temperature and tetragonal at higher temperature expected for LCN around 520 °C [39, 63-65]. However, differing linear thermal expansion coefficients of the monoclinic ($8.6\pm0.5\times10^{-6}$/K) and tetragonal phases (15×10^{-6}/K) could present a challenge for metal support/interconnect materials selection [66-68]. Advantages of MSCs such as rapid startup [17] and dynamic temperature operation [16] could undermined, as micro-cracks may develop in the LCN electrolyte if the temperature ramping rate is too fast or temperature gradients are too large.

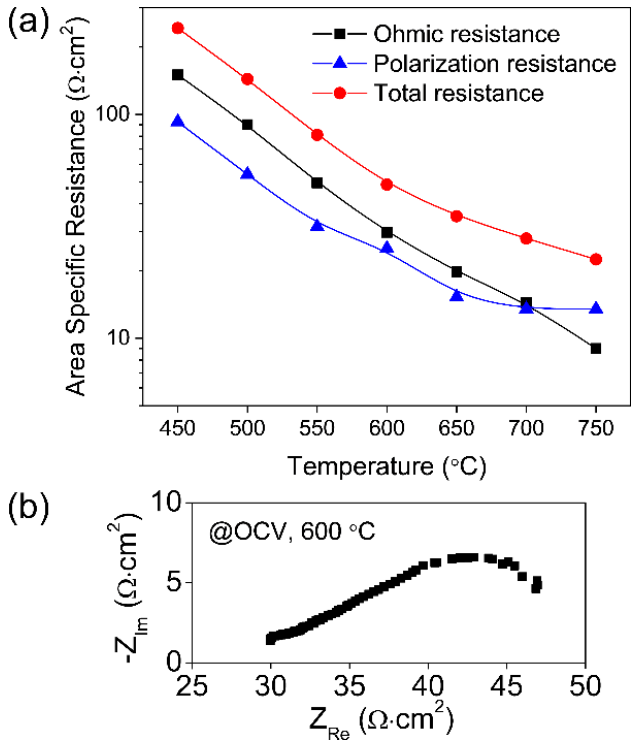

Figure 8. Cell performance. (a) Ohmic, polarization, and total resistance of the LCN-based cell as a function of temperature, with 3% H_2O-H_2 on metal support side and ambient air on Pt side. (b) Impedance spectra measured at 600 °C under open-circuit condition.

4. Conclusions

In this work, representative protonic ceramics including BZCY, SZCY, BCN, LCZ, LCO, and LCN were assessed for viability as the electrolyte material in metal-supported solid oxide cells fabricated by co-sintering. The candidates were screened for compatibility with reducing atmosphere sintering, chemical compatibility with metal support during co-sintering, sintering behavior and evaporation during sintering. LCZ did not survive reducing atmosphere sintering. LCO completely reacted with the metal support. BCN evaporated dramatically and disintegrated into loose powder after sintering. LCZ, LCO, and BCN are therefore concluded to be incompatible with co-sintering fabrication of MSC based on ferritic stainless steel. Although BZCY and SZCY survive the processing conditions and have good ionic conductivity, they partially react with Si and Cr in the metal support, causing formation of secondary phases and Ba/Sr depletion. BZCY also requires a high sintering temperature which limits compatibility with metal support.

Of the candidates studied here, LCN is identified to be the most compatible proton conducting material for co-sintering with metal support, as it can be densified at relatively low temperature (1300 °C), does not evaporate during sintering, and most importantly does not react with the metal support. A metal-supported single cell with LCN electrolyte was successfully fabricated by co-sintering and preliminary electrochemical testing was performed. The cell ohmic impedance

is consistent with the reported conductivity of LCN and is too high to be practical for fuel cell or electrolysis cell application. The impact of the LCN phase transition requires further investigation. Further optimization of the cell should include reduction of electrolyte thickness, improvement of electrolyte conductivity, and optimization of the electrodes.

ACKNOWLEDGEMENTS

The authors gratefully acknowledge Grace Lau for the technical support, and Tianli Zhu and John Yamanis for helpful discussion. This work was made possible through the HydroGEN consortium, which is funded by the U.S. Department of Energy, Office of Energy Efficiency and Renewable Energy, Fuel Cell Technologies Office under Award No. DE-EE0008080 in support of United Technologies Research Center. This work was supported in part by the U.S. Department of Energy, Office of Science, Office of Workforce Development for Teachers and Scientists (WDTS) under the Science Undergraduate Laboratory Internship (SULI) program. This work was funded in part by the U.S. Department of Energy under contract no. DE-AC02-05CH11231. The views and opinions of the authors expressed herein do not necessarily state or reflect those of the United States Government or any agency thereof. Neither the United States Government nor any agency thereof, nor any of their employees, makes any warranty, expressed or implied, or assumes any legal liability or responsibility for the accuracy, completeness, or usefulness of any information, apparatus, product, or process disclosed, or represents that its use would not infringe privately owned rights.

References

[1] E. Fabbri, D. Pergolesi, E. Traversa, Materials challenges toward proton-conducting oxide fuel cells: a critical review, Chem. Soc. Rev. 39 (2010) 4355-4369.

[2] E. Fabbri, L. Bi, D. Pergolesi, E. Traversa, Towards the next generation of solid oxide fuel cells operating below 600 °C with chemically stable proton-conducting electrolytes, Adv. Mater. 24 (2012) 195-208.

[3] L. Bi, S. Boulfrad, E. Traversa, Steam electrolysis by solid oxide electrolysis cells (SOECs) with proton-conducting oxides, Chem. Soc. Rev. 43 (2014) 8255-8270.

[4] J. Phair, S. Badwal, Review of proton conductors for hydrogen separation, Ionics 12 (2006) 103-115.

[5] S. Hossain, A. M. Abdalla, S. N. B. Jamain, J. H. Zaini, A. K. Azad, A review on proton conducting electrolytes for clean energy and intermediate temperature-solid oxide fuel cells, Renewable Sustainable Energy Rev. 79 (2017) 750-764.

[6] K. D. Kreuer, Proton-conducting oxides, Annu. Rev. Mater. Res. 33 (2003) 333-359.

[7] F. Lefebvre-Joud, G. Gauthier, J. Mougin, Current status of proton-conducting solid oxide fuel cells development, J. Appl. Electrochem. 39 (2009) 535-543.

[8] O. Paschos, J. Kunze, U. Stimming, F. Maglia, A review on phosphate based, solid state, protonic conductors for intermediate temperature fuel cells, J. Phys.: Condens. Matter 23 (2011) 234110.

[9] R. Reijers, W. Haije, Literature review on high temperature proton conducting materials, Energy research Centre of the Netherlands, (2008) 08.

[10] C. Duan, R. J. Kee, H. Zhu, C. Karakaya, Y. Chen, S. Ricote, A. Jarry, E. J. Crumlin, D. Hook, R. Braun, Highly durable, coking and sulfur tolerant, fuel-flexible protonic ceramic fuel cells, Nature 557 (2018) 217.

[11] L. Yang, S. Wang, K. Blinn, M. Liu, Z. Liu, Z. Cheng, M. Liu, Enhanced sulfur and coking tolerance of a mixed ion conductor for SOFCs: $BaZr_{0.1}Ce_{0.7}Y_{0.2-x}Yb_xO_{3-\delta}$, Science 326 (2009) 126-129.

[12] S. Giddey, S. Badwal, A. Kulkarni, Review of electrochemical ammonia production technologies and materials, Int. J. Hydrogen Energy 38 (2013) 14576-14594.

[13] H. Matsumoto, S. Hamajima, H. Iwahara, Electrochemical hydrogen pump using a high-temperature-type proton conductor: improvement of pumping capacity, Solid State Ionics 145 (2001) 25-29.

[14] Z. Tao, L. Yan, J. Qiao, B. Wang, L. Zhang, J. Zhang, A review of advanced proton-conducting materials for hydrogen separation, Prog. Mater. Sci. 74 (2015) 1-50.

[15] K. Xie, Y. Zhang, G. Meng, J. T. Irvine, Electrochemical reduction of CO_2 in a proton conducting solid oxide electrolyser, J. Mater. Chem. 21 (2011) 195-198.

[16] M. C. Tucker, Dynamic-temperature operation of metal-supported solid oxide fuel cells, J. Power Sources 395 (2018) 314-317.

[17] M. C. Tucker, A. S. Ying, Metal-supported solid oxide fuel cells operated in direct-flame configuration, Int. J. Hydrogen Energy 42 (2017) 24426-24434.

[18] M. C. Tucker, Durability of symmetric-structured metal-supported solid oxide fuel cells, J. Power Sources, 369 (2017) 6-12.

[19] R. T. Leah, A. Bone, E. Hammer, A. Selcuk, M. Rahman, A. Clare, S. Mukerjee, M. Selby, Development Progress on the Ceres Power Steel Cell Technology Platform: Further Progress Towards Commercialization, ECS Trans. 78 (2017) 87-95.

[20] M. C. Tucker, Personal power using metal-supported solid oxide fuel cells operated in a camping stove flame, Int. J. Hydrogen Energy 43 (2018) 8991-8998.

[21] M. C. Tucker, B. Carreon, J. Charyasatit, K. Langston, C. Taylor, J. Manjarrez, N. Burton, M. LaBarbera, C. P. Jacobson, Playing with Fire: Commercialization of a Metal-Supported SOFC Product for Use in Charcoal Cookstoves for the Developing World, ECS Trans. 78 (2017) 229-236.

[22] M. C. Tucker, Development of High Power Density Metal-Supported Solid Oxide Fuel Cells, Energy Technol. 5 (2017) 2175-2181.

[23] D. Udomsilp, D. Roehrens, N. Menzler, C. Bischof, L. de Haart, A. Opitz, O. Guillon, M. Bram, High-Performance Metal-Supported Solid Oxide Fuel Cells by Advanced Cathode Processing, J. Electrochem. Soc. 164 (2017) F1375-F1384.

[24] J. Nielsen, A. H. Persson, T. T. Muhl, K. Brodersen, Towards High Power Density Metal Supported Solid Oxide Fuel Cell for Mobile Applications, J. Electrochem. Soc. 165 (2018) F90-F96.

[25] G. Schiller, A. Ansar, M. Lang, O. Patz, High temperature water electrolysis using metal supported solid oxide electrolyser cells (SOEC), J. Appl. Electrochem. 39 (2009) 293-301.

[26] T. Chen, Y. Zhou, M. Liu, C. Yuan, X. Ye, Z. Zhan, S. Wang, High performance solid oxide electrolysis cell with impregnated electrodes, Electrochem. Commun. 54 (2015) 23-27.

[27] R. Wang, E. Dogdibegovic, G. Y. Lau, M. C. Tucker, Metal-Supported Solid Oxide Electrolysis Cell (MS-SOEC) With Significantly Enhanced Catalysis, submitted.

[28] M. C. Tucker, Progress in metal-supported solid oxide fuel cells: A review, J. Power Sources 195 (2010) 4570-4582.

[29] Y. Larring, M. L. Fontaine, Critical issues of metal-supported fuel cell, in: J. T. S. Irvine, P. Connor (Eds.), Solid Oxide Fuels Cells: Facts and Figures, Springer, London, 2013, pp. 71-93.

[30] V. V. Krishnan, Recent developments in metal-supported solid oxide fuel cells, Wiley Interdiscip. Rev.: Energy Environ. 6 (2017) e246.

[31] E. Dogdibegovic, R. Wang, G. Y. Lau, M. C. Tucker, High Performance Metal-Supported Solid Oxide Fuel Cells with Infiltrated Electrodes, J. Power Sources 410 (2019) 91-98.

[32] E. Mercadelli, A. Gondolini, P. Pinasco, A. Sanson, S. Barison, M. Fabrizio, Key Issues in Processing Metal-Supported Proton Conducting Anodes for SOFCs Applications, ECS Trans. 35 (2011) 1761-1769.

[33] M. Stange, E. Stefan, C. Denonville, Y. Larring, P. Rørvik, R. Haugsrud, Development of novel metal-supported proton ceramic electrolyser cell with thin film BZY15–Ni electrode and BZY15 electrolyte, Int. J. Hydrogen Energy 42 (2017) 13454-13462.

[34] E. Stefan, M. Stange, C. Denonville, Y. Larring, N. Hildenbrand, T. Norby, R. Haugsrud, Layered microstructures based on $BaZr_{0.85}Y_{0.15}O_{3-\delta}$ by pulsed laser deposition for metal-supported proton ceramic electrolyser cells, J. Mater. Sci. 52 (2017) 6486-6497.

[35] S. Choi, C. J. Kucharczyk, Y. Liang, X. Zhang, I. Takeuchi, H. I. Ji, S. M. Haile, Exceptional power density and stability at intermediate temperatures in protonic ceramic fuel cells, Nat. Energy 3 (2018) 202.

[36] Y. Yamazaki, R. Hernandez-Sanchez, S. M. Haile, High total proton conductivity in large-grained yttrium-doped barium zirconate, Chem. Mater. 21 (2009) 2755-2762.

[37] K. Leonard, Y. S. Lee, Y. Okuyama, K. Miyazaki, H. Matsumoto, Influence of dopant levels on the hydration properties of SZCY and BZCY proton conducting ceramics for hydrogen production, Int. J. Hydrogen Energy 42 (2017) 3926-3937.

[38] T. Omata, S. Otsuka-Yao-Matsuo, Electrical properties of proton-conducting Ca^{2+}-doped $La_2Zr_2O_7$ with a pyrochlore-type structure, J. Electrochem. Soc. 148 (2001) E252-E261.

[39] R. Haugsrud, T. Norby, Proton conduction in rare-earth ortho-niobates and ortho-tantalates, Nat. Mater. 5 (2006) 193.

[40] W. Sun, S. Fang, L. Yan, W. Liu, Investigation on proton conductivity of $La_2Ce_2O_7$ in wet atmosphere: dependence on water vapor partial pressure, Fuel Cells 12 (2012) 457-463.

[41] R. Haugsrud, T. Norby, High-Temperature Proton Conductivity in Acceptor-Substituted Rare-Earth Ortho-Tantalates, $LnTaO_4$, J. Am. Ceram. Soc. 90 (2007) 1116-1121.

[42] H. L. Ray, N. Zhao, L. C. De Jonghe, Hole percolation and proton conduction in monazite solid solutions: $La_{0.98-x}Ce_xSr_{0.02}PO_{4-\delta}$, Electrochim. Acta 78 (2012) 294-301.

[43] S. Wang, F. Zhao, L. Zhang, K. Brinkman, F. Chen, Doping effects on complex perovskite $Ba_3Ca_{1.18}Nb_{1.82}O_{9-\delta}$ intermediate temperature proton conductor, J. Power Sources 196 (2011) 7917-7923.

[44] C. Duan, J. Tong, M. Shang, S. Nikodemski, M. Sanders, S. Ricote, A. Almansoori, R. O'Hayre, Readily processed protonic ceramic fuel cells with high performance at low temperatures, Science 349 (2015) 1321-1326.

[45] H. An, H. W. Lee, B. K. Kim, J. W. Son, K. J. Yoon, H. Kim, D. Shin, H. I. Ji, J. H. Lee, A 5× 5 cm^2 protonic ceramic fuel cell with a power density of 1.3 W cm^{-2} at 600 °C, Nat. Energy 3 (2018) 870.

[46] http://www.cerpotech.com/?q=products/barium-cerium-yttrium-zirconate-bzcy.

[47] M. C. Tucker, G. Y. Lau, C. P. Jacobson, L. C. DeJonghe, S. J. Visco, Performance of metal-supported SOFCs with infiltrated electrodes, J. Power Sources 171 (2007) 477-482.

[48] T. Z. Sholklapper, V. Radmilovic, C. P. Jacobson, S. J. Visco, L. C. De Jonghe, Synthesis and stability of a nanoparticle-infiltrated solid oxide fuel cell electrode, Electrochem. Solid-State Lett. 10 (2007) B74-B76.

[49] L. Bi, E. Fabbri, E. Traversa, Solid oxide fuel cells with proton-conducting $La_{0.99}Ca_{0.01}NbO_4$ electrolyte, Electrochim. Acta 260 (2018) 748-754.

[50] Y. Ling, J. Chen, Z. Wang, C. Xia, R. Peng, Y. Lu, New ionic diffusion strategy to fabricate proton-conducting solid oxide fuel cells based on a stable $La_2Ce_2O_7$ electrolyte, Int. J. Hydrogen Energy 38 (2013) 7430-7437.

[51] L. Bi, S. Zhang, S. Fang, L. Zhang, H. Gao, G. Meng, W. Liu, In Situ Fabrication of a Supported $Ba_3Ca_{1.18}Nb_{1.82}O_{9-\delta}$ Membrane Electrolyte for a Proton-Conducting SOFC, J. Am. Ceram. Soc. 91 (2008) 3806-3809.

[52] A. Magrasó, M. L. Fontaine, Y. Larring, R. Bredesen, G. Syvertsen, H. Lein, T. Grande, M. Huse, R. Strandbakke, R. Haugsrud, Development of proton conducting SOFCs based on $LaNbO_4$ electrolyte–status in Norway, Fuel Cells 11 (2011) 17-25.

[53] A. Magrasó, M. L. Fontaine, R. Bredesen, R. Haugsrud, T. Norby, Cathode compatibility, operation, and stability of $LaNbO_4$-based proton conducting fuel cells, Solid State Ionics 262 (2014) 382-387.

[54] A. Magrasó, H. Xuriguera, M. Varela, M. F. Sunding, R. Strandbakke, R. Haugsrud, T. Norby, Novel Fabrication of Ca-Doped $LaNbO_4$ Thin-Film Proton-Conducting Fuel Cells by Pulsed Laser Deposition, J. Am. Ceram. Soc. 93 (2010) 1874-1878.

[55] E. Fabbri, A. D'Epifanio, E. Di Bartolomeo, S. Licoccia, E. Traversa, Tailoring the chemical stability of $Ba(Ce_{0.8-x}Zr_x)Y_{0.2}O_{3-\delta}$ protonic conductors for intermediate temperature solid oxide fuel cells (IT-SOFCs), Solid State Ionics 179 (2008) 558-564.

[56] T. Sakai, S. Matsushita, H. Matsumoto, S. Okada, S. Hashimoto, T. Ishihara, Intermediate temperature steam electrolysis using strontium zirconate-based protonic conductors, Int. J. Hydrogen Energy 34 (2009) 56-63.

[57] Y. H. Xie, J. D. Wang, R. Q. Liu, X. T. Su, Z. P. Sun, Z. J. Li, Preparation of $La_{1.9}Ca_{0.1}Zr_2O_{6.95}$ with pyrochlore structure and its application in synthesis of ammonia at atmospheric pressure, Solid State Ionics 168 (2004) 117-121.

[58] B. Lin, S. Wang, X. Liu, G. Meng, Stable proton-conducting Ca-doped $LaNbO_4$ thin electrolyte-based protonic ceramic membrane fuel cells by in situ screen printing, J. Alloys Compd. 478 (2009) 355-357.

[59] T. Mokkelbost, Ø. Andersen, R. A. Strøm, K. Wiik, T. Grande, M. A. Einarsrud, High-Temperature Proton-Conducting $LaNbO_4$-Based Materials: Powder Synthesis by Spray Pyrolysis, J. Am. Ceram. Soc. 90 (2007) 3395-3400.

[60] P. Babilo, T. Uda, S. M. Haile, Processing of yttrium-doped barium zirconate for high proton conductivity, J. Mater. Res. 22 (2007) 1322-1330.

[61] Y. Yamazaki, R. Hernandez-Sanchez, S. M. Haile, Cation non-stoichiometry in yttrium-doped barium zirconate: phase behavior, microstructure, and proton conductivity, J. Mater. Chem. 20 (2010) 8158-8166.

[62] S. Nikodemski, J. Tong, R. O'Hayre, Solid-state reactive sintering mechanism for proton conducting ceramics, Solid State Ionics 253 (2013) 201-210.

[63] L. Malavasi, C. Ritter, G. Chiodelli, Investigation of the high temperature structural behavior of $La_{0.99}Ca_{0.01}NbO_4$ proton conducting material, J. Alloys Compd. 475 (2009) L42-L45.

[64] A. Magrasó, R. Haugsrud, T. Norby, Preparation and Characterization of Ni–$LaNbO_4$ Cermet Anode Supports for Proton-Conducting Fuel Cell Applications, J. Am. Ceram. Soc. 93 (2010) 2650-2655.

[65] L. Jian, C. Wayman, Monoclinic-to-Tetragonal Phase Transformation in a Ceramic Rare-Earth Orthoniobate, $LaNbO_4$, J. Am. Ceram. Soc. 80 (1997) 803-806.

[66] T. Norby, A. Magrasó, On the development of proton ceramic fuel cells based on Ca-doped $LaNbO_4$ as electrolyte, J. Power Sources 282 (2015) 28-33.

[67] T. Mokkelbost, H. L. Lein, P. E. Vullum, R. Holmestad, T. Grande, M. A. Einarsrud, Thermal and mechanical properties of $LaNbO_4$-based ceramics, Ceram. Int. 35 (2009) 2877-2883.

[68] A. W. B. Skilbred, R. Haugsrud, Sandvik Sanergy HT–A potential interconnect material for $LaNbO_4$-based proton ceramic fuel cells, J. Power Sources 206 (2012) 70-76.